Sensitivity of stratospheric dynamics to uncertainty in O_3 production

Juno Hsu,[1] Michael J. Prather,[1] Dan Bergmann,[2] and Philip Cameron-Smith[2]

Received 11 June 2012; revised 26 July 2013; accepted 30 July 2013; published 29 August 2013.

[1] Some key photochemical uncertainties that cannot be readily eliminated by current observations translate into a range of stratospheric O_3 abundances in the tens of percent. The uncertainty in O_3 production due to that in the cross sections for O_2 in the Hertzberg continuum is studied here with the NCAR Community Atmosphere Model, which allows for interactive climate and ozone chemistry. A min-max range in the O_2 cross sections of 30%, consistent with current uncertainties, changes O_3 abundances in the lower tropical stratosphere by up to 30%, with a relatively smaller and opposite change above 30 hPa. Here we have systematically examined the changes in the time-mean state, the seasonal cycle, and the interannual variability of the temperature and circulation associated with the ±30% change in O_2 cross sections. This study points to the important role of O_3 in the lower tropical stratosphere in determining the physical characteristics of the tropical tropopause layer. Reducing O_2 cross sections by 30% increases ozone abundances which warms the lower stratosphere (60°S –60°N; 2 K maximum at equator) and lowers the tropopause height by 100–200 m (30°S –30°N). The large-scale warming leads to enhanced stratification near the tropopause which reduces upward wave propagation everywhere except for high latitudes. The lowermost tropical stratosphere is better ventilated during austral winter. The annual cycle of ozone is amplified. The interannual variability of the winter stratospheric polar vortices also increases, but the mechanism involves wave-mean flow interaction, and the exact role of ozone in it needs further investigation.

Citation: Hsu, J., M. J. Prather, D. Bergmann, and P. Cameron-Smith (2013), Sensitivity of stratospheric dynamics to uncertainty in O_3 production, *J. Geophys. Res. Atmos.*, *118*, 8984–8999, doi:10.1002/jgrd.50689.

1. Introduction

[2] Tremendous progress has been made in separate studies of atmospheric chemistry, stratospheric dynamics, and climate change. Yet, how uncertainties propagate through these components has not been adequately addressed. This is an urgent issue since predicting future climate change requires assessing the range of uncertainties that result from interactions among all components of the Earth System. In this study, we focus on the impact of uncertainties in the photochemistry of ozone on stratospheric dynamics. We use an atmospheric chemistry-climate model to calculate specifically how current uncertainties in the primary photochemical production of O_3 can change ozone abundances in the lower tropical stratosphere and, through radiative adjustment, change the dynamical basic state and variability.

[3] In their ozone assessment study, *Eyring et al.* [2006] show that although the majority of the 13 participating chemistry-climate models (CCMs) agree with each other, there are nevertheless substantial differences in the ozone distributions of the state-of-the-art CCMs. For example, the model range of the climatological equatorial ozone abundances at 50 hPa is about 1–3 ppm (μmol/mol) while the observed climatological value is about 1.6±0.2 ppm, derived from the HALOE data. The peak values of the total column ozone climatology in March at high latitudes vary from 350 DU to 550 DU across models while the mean observed value from the merged TOMS and SBUV2 satellite data set is about 425 DU [see *Eyring et al.*, 2006, Figures 13(d) and 14]. Ozone biases are often the result of errors in the temperature and circulation in the models, and even with standardization of the chemical rates, there remain errors in chemistry implementation. Biases in temperature affect ozone through temperature-dependent chemical reaction rates in both gas and heterogeneous chemistry. A model with positive temperature bias in the stratosphere would overestimate ozone destruction through the gas-phase reactions but underestimate the extent of ozone depletion through Polar Stratospheric Clouds (PSCs). A slower Brewer-Dobson circulation (BDC) leads to larger ozone abundances in

Additional supporting information may be found in the online version of this article.

[1]Department of Earth System Science, University of California, Irvine, California, USA.

[2]Lawrence Livermore National Laboratory, Livermore, California, USA.

Corresponding author: J. Hsu, Department of Earth System Science, University of California, Irvine, CA 92697, USA. (junoh@uci.edu)

2169-897X/13/10.1002/jgrd.50689

the tropics and smaller abundances in midlatitudes. The problem of how ozone biases feedback on the temperature and circulation of the models, however, has not received much attention.

[4] Ozone, a major UV-radiation absorber, sets the thermal structure of the stratosphere. The overturning circulation of the stratosphere is driven, however, not thermally but by waves [*Holton et al.*, 1995]. Without the wave drag contributed from planetary waves and small-scale gravity waves, the stratosphere would be close to its radiative equilibrium state with the large-scale circulation in thermal wind balance [*Andrew et al.*, 1987]. Dissipation of waves acts as a mechanical pump to induce the thermally indirect Brewer-Dobson residual circulation, which rises from the equator and sinks in the extratropics (for a review of the middle atmosphere, see *Shepherd* [2000]). Planetary wave propagation and its dissipation in the stratosphere, however, owe their own existence to the mechanical and thermal structures of the background mean state, which ozone maintains in the first place. Errors in the ozone simulation can, in principle, propagate into the dynamical forcing.

[5] Examples of stratospheric ozone change influencing the dynamics of the atmosphere are many. Over the last three decades, ozone depletion has been implicated in changes in not only the atmospheric circulation [*Li et al.*, 2008; *Lee and Feldstein*, 2013] but also ocean circulation [*Cai and Cowan*, 2007; *Waugh et al.*, 2013]. *Fueglistaler et al.* [2011] found that the seasonal variation of tropical ozone contributes to the prominent annual cycle of temperature in the lower tropical stratosphere near 70 hPa, modifying the long-standing view that the lower stratospheric temperature is solely controlled by the annual cycle of the BDC [*Yulaeva et al.*, 1994; *Ueyama and Wallace*, 2010]. *Chen and Robinson* [1992] pointed out that the upward propagation of planetary waves to the stratosphere is sensitive to the vertical gradient of buoyancy frequency squared (N^2) at the tropopause, which acts as a valve for wave propagation. Through radiative heating, the lower stratospheric ozone variability can produce such an enhanced N^2 gradient at the tropopause [*Nakamura et al.*, 2009]. Here we show that the uncertainty in the primary production of ozone, effectively a systematic bias in stratosphere, can also impede upward wave propagation and change poleward eddy heat fluxes in the stratosphere by changing the vertical N^2 gradient.

[6] In this study, we examine the stratospheric climate statistics from alternative stratospheric O_3 chemistry, defined by the uncertainty range in O_2 cross sections, within the Community Atmosphere Model version 5 (CAM5 hereafter) [*Gettelman et al.*, 2012]. Stratospheric ozone is simulated by Linoz (Linearized stratospheric ozone) version 2 [*Hsu and Prather*, 2009]. This CAM-Linoz model is self-consistent in that the circulation determines stratosphere O_3, and this O_3 is used in the radiative calculation that forces the circulation. Within the range of ozone chemistry, we select the uncertainty in the O_2 photolysis cross sections in the Herzberg continuum [*Sander et al.*, 2011]. In our reference model, we use the canonical laboratory cross-section measurements [*Yoshino et al.*, 1988], and in our uncertainty cases, we reduce or increase these values by 30% over the wavelengths 202–242 nm as an estimate of 90% confidence interval in these cross sections based on the uncertainty factor 1.2 in *Sander et al.* [2011] with 20% being interpreted as 1-σ uncertainty from the mean. The Herzberg photolysis of O_2 dominates production of O_3 throughout the lower stratosphere and even reaches into the upper tropical troposphere [*Prather*, 2009]. The model and simulation setup are further explained in section 2. Results are presented in section 3, followed by a discussion and conclusions in section 4.

2. CAM 5 With Interactive Ozone Simulated With Linoz v2

2.1. Numerical Simulations

[7] We use CAM5, the atmospheric component of the Community Earth System Model CESM 1.0, coupled to Linoz v2 [*Hsu and Prather*, 2009] so as to include the radiative feedback of stratospheric O_3. Our configuration has 144 longitudinal × 96 latitudinal grid cells with a resolution of 2.5° in longitude and ∼1.9° in latitude. There are 30 vertical levels with the vertical resolution ∼1 km from the middle troposphere to the lowermost stratosphere (500 hPa to 80 hPa) represented by 12 model levels, and about ∼2 km resolution up to 45 hPa, and increasing up to ∼5 km for the top three levels ending at 2 hPa. Our focus is primarily on large-scale changes in temperature and circulation due to changes in ozone chemistry. Most of the changes occur in the lower stratosphere where the vertical resolution of 1–2 km is deemed adequate, because changes in tropopause height and N^2 are detectable when comparing the model runs (see section 3).

[8] Linoz is a stratospheric ozone photochemical scheme obtained by linearizing the net ozone photochemical production (P-L) about the climatological state using a first-order Taylor expansion in terms of ozone abundances, overhead column ozone (UV radiation), and temperature. The reference ozone production and derivatives used in Linoz are obtained by running a photochemical box model [*Prather*, 1992], which includes complete and up-to-date non-PSC stratospheric chemistry. PSC chemistry is parameterized with the Cariolle method [*Cariolle et al.*, 1990] and produces a reasonable ozone hole. We tabulate Linoz terms as a function of latitude, month, and height so that the chemistry is effectively averaged over each CAM5 layer. Note that Linoz v2 has only one prognostic variable, ozone. All other long-lived tracers such as N_2O, NO_y, or CH_4 are assumed to remain at their assigned climatological abundances and provide no further interactive feedback to ozone simulation in CAM5. Nevertheless, all Cly- , Bry-, NOx- and HOx-catalyzed chemistry are present in deriving the net ozone production rate and its derivatives.

[9] Linoz has been used in the UCI CTM model driven by ECMWF-IFS data to study stratospheric ozone variability and the ozone fluxes crossing the tropopause [*Hsu et al.*, 2005; *Hsu and Prather*, 2009] and to hindcast the Aura satellite observations [*Tang and Prather*, 2010, 2012]. Linoz v2 is an update of a previous version [*McLinden et al.*, 2000], with JPL-2010 chemical kinetic rates, improved ozone climatology profiles and solar fluxes. The latitude-height profiles for inorganic chlorine (Cly), bromine (Bry), reactive nitrogen (NOy), and water vapor are obtained using the observed tracer-tracer correlations. Their profiles

Table 1. List of Model Simulations With CAM5-Linoz v2[a]

Runs	Troposphere	Stratosphere	Years Analyzed
Sfast-Ctrl	LLNL Superfast Chemistry + limited aerosol-cloud interaction[a]	standard Linoz	10
Sfast-O2jr	LLNL Superfast Chemistry+ limited aerosol-cloud interaction[a]	Linoz-O2jr[b]	10
Mozart-Ctrl	Mozart-Chemistry	Standard Linoz	25
Mozart-O2jr	Mozart-Chemistry	Linoz-O2jr [b]	25
Mozart-O2ji	Mozart-Chemistry	Linoz-O2ji [c]	25

[a]Aerosols from Surperfast-Chemistry were not used in cloud-aerosol interaction. Only minimal aerosols from the cloud subroutines were used.
[b]Linoz-O2jr is generated with 0.7* O_2 cross sections within the Hertzberg Continuum (202–240 nm).
[c]Linoz-O2ji is generated with 1.3* O_2 cross sections within the Hertzberg Continuum (202–240 nm).

are scaled to the assigned surface abundances of N_2O, halocarbons, and CH_4 (see Section 2 of *Hsu and Prather* [2009] for details). In this study, Linoz ozone tables are generated with long-lived tracers prescribed at the year 2000 of the IPCC-AR5 scenario [*IPCC*, 2007]: surface N_2O (316 ppb (nmol/mol)), maximum NO_y (19.2 ppb), maximum Cl_y (3428 ppt (pmol/mol)), and maximum Br_y (16.5 ppt), and CH_4 (1760 ppb). The standard table, Linoz-Ctrl, is generated without any modification while the alternative table, Linoz-O2jr, is generated with the O_2 cross sections reduced by 30% between 202 nm and 240 nm, and the table, Linoz-O2ji, is generated with O_2 cross sections increased by 30% for the same wavelength range.

[10] Table 1 summarizes the five numerical simulations conducted in this study. These consist two sets of control and perturbation experiments with the sets labeled as Mozart- and Sfast- runs. Three Mozart runs (Mozart-Ctrl, Mozart-O2jr, and Mozart-O2ji) use the standard Mozart tropospheric chemistry package [*Lamarque et al.*, 2012], while the two Super-fast Chemistry runs (Sfast-Ctrl and Sfast-O2jr) use a simplified version of the LLNL-IMPACT tropospheric chemistry scheme [*Rotman et al.*, 2004] as described in *Cameron-Smith et al.* [2006], *Lamarque et al.* [2013], and *Stevenson et al.* [2013]. For our focus on stratospheric ozone and dynamics, the choice of tropospheric chemistry scheme is a secondary influence on the model's response. Here the uncertainty in the O_2 cross sections applies *only* to the stratospheric chemistry (Linoz v2), not the tropospheric chemistry (Sfast or Mozart). There is one important difference in the model configuration that sets these two sets of simulations

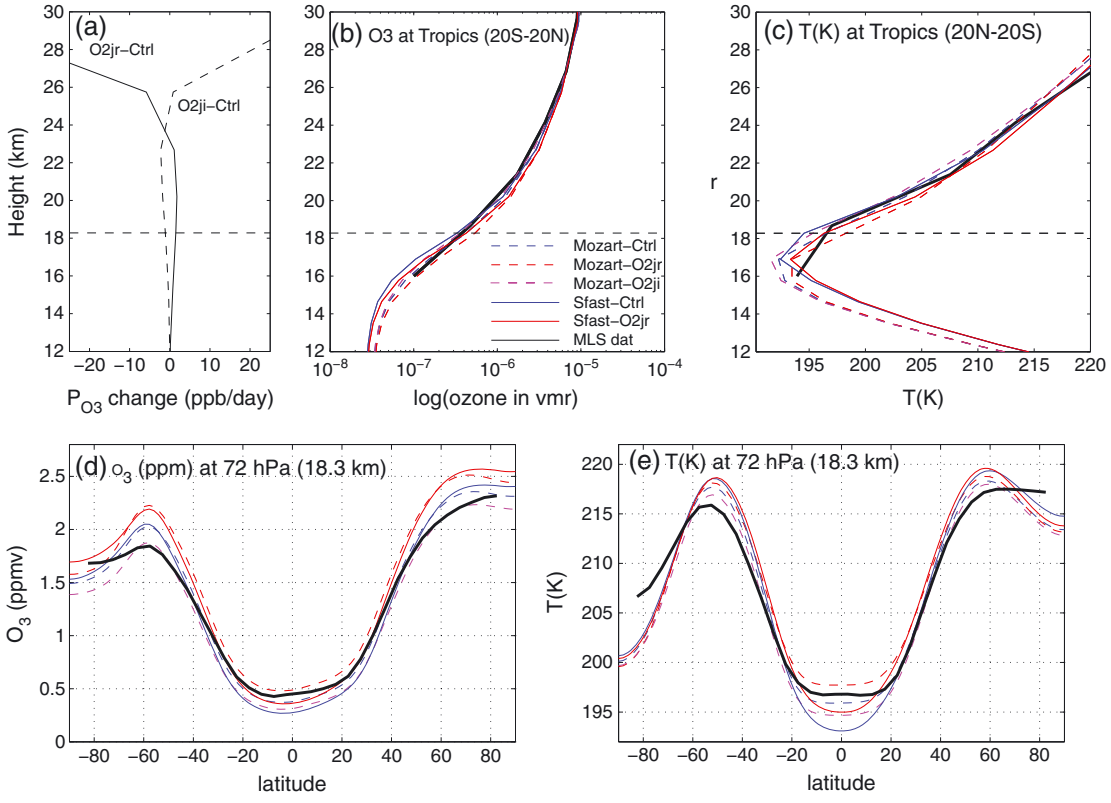

Figure 1. Vertical profiles as a function of pressure altitude (height $z^* = 16 \times \log10(1000/P)$) of the following: (a) changes in O_3 photochemical production (ppb/day) for a –30% change in O_2 cross section (O2jr-Ctrl, solid) and a +30% change (O2ji-Ctrl, dashed); (b) tropical (20 °S–20 °N) multi-year annual means of O_3 (ppm); (c) same for temperature (K). Latitudinal profiles at 72 hPa (18.3 km) of (d) O_3 (ppm) and (e) temperature (K). The 72 hPa level is noted in Figures 1a–1c.

apart. The cloud model in CAM5 uses cloud condensation nuclei (CCN) based on the aerosols in the model, however, due to a bug in the version of CAM5 used for the Sfast simulations, the aerosols were not communicated to the cloud nucleation routine. This bug was fixed for our Mozart runs. As a result, the basic climate and time-mean temperature are quite different between Mozart-Ctrl and Sfast-Ctrl. Thus, the two sets of the ctrl-perturbation simulations cannot be treated as two ensembles of the same experiment, but rather as a multimodel ensemble, i.e., the same chemical perturbation applied to two different climate states.

[11] For all five simulations, the year 2000 climate is simulated with prescribed greenhouse gases and observed sea surface temperatures (SST) representative of this period. The surface boundary conditions are annually repeating, and all simulations are spun up for 4–5 years, which is adequate with fixed SSTs. Only monthly zonal mean data after the spin-up are analyzed: 10 years for Sfast runs and 25 years for Mozart runs. The mean and variance of six climate variables are analyzed and presented: ozone abundances, temperature, zonal wind, solar heating, the mass stream function, and eddy forcing. Eddy forcing (or wave drag) is calculated as the divergence of E-P fluxes based on *Andrew et al.* [1987, Equations 3.5.3a and 3.5.3b]. The mass stream function shown in this study is calculated from vertically integrating the residual meridional velocity vertically as in *McLandress and Shepherd* [2009, Equation 2].

[12] A Bayesian method is used to quantify the uncertainty of some of the results, particularly of the mean of the climate variables (e.g., those shown in Figure 2) and the mean of the temporal variances (i.e., the interannual temperature variances in Figure 10). To estimate the mean of a climate variable and its uncertainty, we assume the variable is normally distributed. The error bar (1-σ) for the mean value of a normally distributed variable is simply the standard deviation of the time series divided by the square root of the number of independent samples (degree of freedom). To estimate the mean of the variances and the uncertainty of this mean, we use the Bayes theorem to compute the posterior probability density function (pdf) of a parameter, κ (defined below). The posterior pdf is proportional to the product of the likelihood function and the prior probability function for κ. The functional form of the likelihood function we used is equivalent to the chi-squared, $\chi^2(x;\nu)$ pdf with a change of variables with x and ν rescaled by the mean variance, σ^2, we wish to estimate. The resulting dimensional parameter $\kappa \equiv \nu \cdot \sigma^2$ controls the shape of the pdf and is equal to its expected value. Thus, it represents the mean value of the variances. For the prior probability density function for κ, we used a flat prior. An example from analyzing a time series of temperature variances is provided in Figure S1 of the supporting information. As seen in Figure S1(d), the χ^2 curve calculated with the most probable value of κ (from Figure S1(c)) captures the shape of the normalized data histogram (bar graphs) well. For a complete tutorial of the Bayesian method, see the textbook *Sivia and Skilling* [2006].

2.2. Perturbed Ozone Production and Validations Against MLS Data

[13] The difference in the ozone production rates at the equator—Linoz-O2jr minus Linoz-Ctrl, and Linoz-O2ji minus Linoz-Ctrl are illustrated in Figure 1a. When O_2 cross sections are reduced by 30% (i.e., O2jr-Ctrl), the negative change in the upper and middle stratosphere is large (–1000 ppb/day at the top of the model, and –50 ppb/day at 30 km), but it turns positive below 23 km with its maximum value of +1.8 ppb/day at 20 km. This increase throughout the lower stratosphere is due to more UV radiation reaching to the lower stratosphere since there is less UV radiation absorbed aloft as a result of both reduced O_2 cross sections and overhead ozone column. The net change of the total stratospheric column is driven by the lower stratosphere and is positive. The opposite occurs when the O_2 cross sections are increased by 30%. However, the results are not merely a flip of sign from that of O2jr-Ctrl. The magnitude changes are smaller: +880 ppb/day at the top of the model and +34 ppb/day at 30 km. The sign change also occurs at 23 km with the peak rate –2.2 ppb/day at 20 km. At 17 km, for instance, the change in ozone production for O2jr-Ctrl is +1.2 ppb/day but for O2ji-Ctrl is –0.7 ppb/day. As might have been expected, the two opposite changes in O_2 cross sections ($\pm$ 30%) are not comparable because the response of O_3 was more to the relative change than the absolute. The increase was a factor of 1.30, but the decrease (–30%) was a factor of 1.43 (= 1/0.7). Above 30 km, the ratio of the response in O_3 production is about 1.1 (1.43/1.30), 10% larger for O2jr-Ctrl. Below this level, however, the overhead ozone column becomes increasingly important, and the production rates diverge even more from integrating the differences above. Thus, the increased case has a much weaker production rate change in magnitude in the lower stratosphere.

[14] To evaluate the current climate simulated by the CAM5-Linoz v2 combination, we compare the long-term annual mean of the five simulations (Table 1) to 6 years of observations (August 2004–December 2010) from Aura MLS satellite data [*Froidevaux et al.*, 2008; *Schwartz et al.*, 2008]. Figures 1b and 1c show tropical (20°S–20°N) profiles of ozone and temperature from multiyear annual averages, while Figures 1d and 1e show similarly averaged latitudinal structures at 72 hPa (18.3 km). Throughout the stratosphere (19–30 km), the MLS tropical ozone abundances are at the lower range of the model simulations, but this reverses below 18 km. At the level, 72 hPa (Figure 1d), the MLS ozone are above Mozart-Ctrl in tropics, but closely follow Mozat-Ctrl poleward of 20° and gradually veer toward Mozart-O2ji in midlatitudes. Poleward of 60°, current MLS ozone does not decrease as fast as the simulations, which are prescribed with year 2000 halogen levels. Overall, Linoz chemistry for the most part overestimates stratospheric ozone abundances. The MLS tropical temperatures are matched reasonably well by the models although the models are biased low above 27 km. There are large discrepancies near the tropopause region, but the resolution of MLS is probably inadequate here for such detailed comparison. For other latitudes in the lower stratosphere (Figure 1e), the most notable model-observation differences are the following: the peak temperatures at midlatitudes are about 2–3 K warmer and 5° more equatorward in the CAM5 models than in MLS data, and the former are consistently colder at the poles. Overall, given the coarse vertical resolution in CAM5 in the middle stratosphere and the relatively simple Linoz ozone scheme, CAM5-Linoz v2 captures the primary structures of ozone and temperature representative of the current climate.

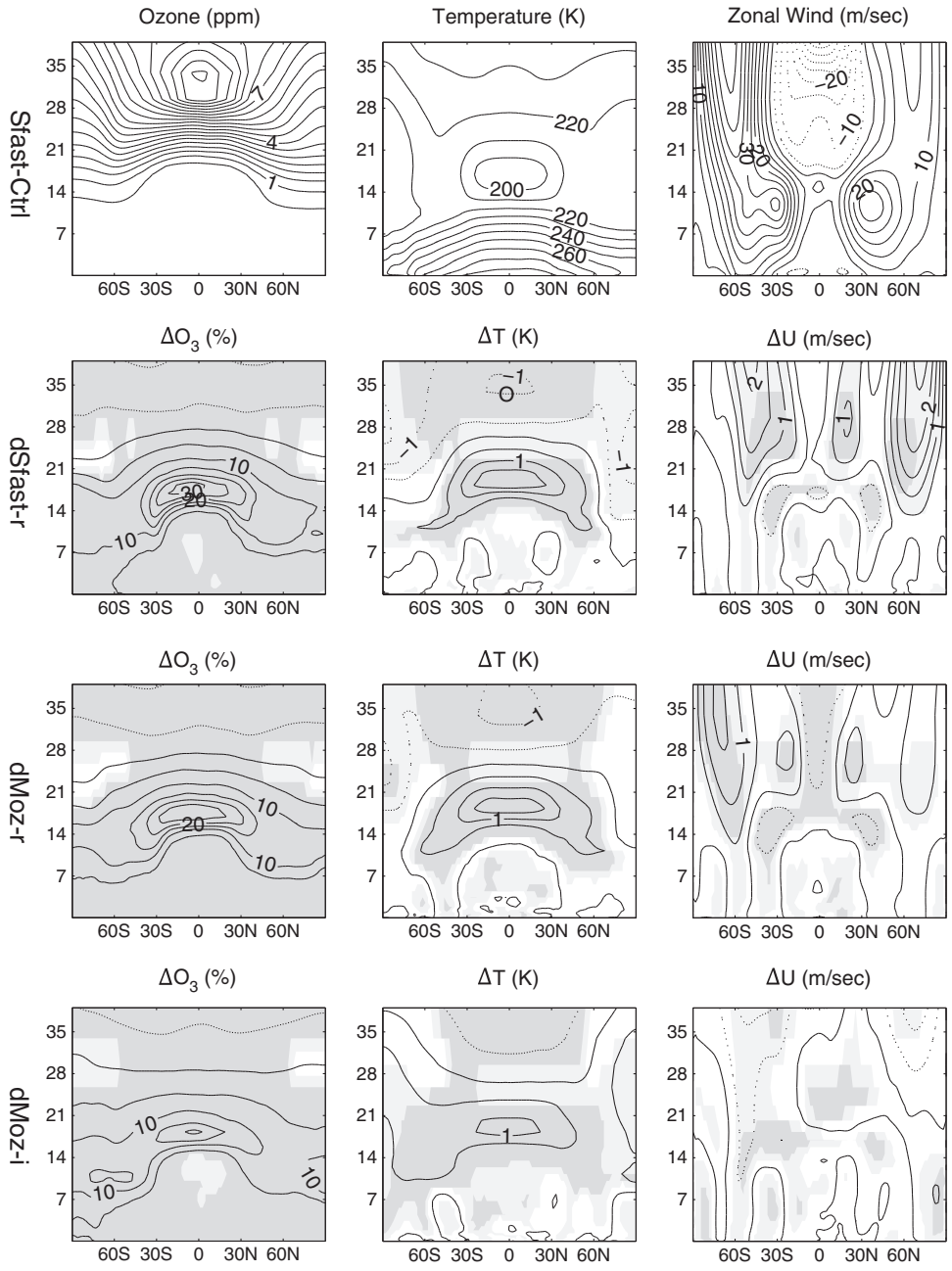

Figure 2. (top) The annual mean states for the Sfast-Ctrl run: ozone (O_3), temperature (T), and the zonal wind (U). Contour interval is 0.5 ppm for ozone, 10 K for temperature and 5 m/sec for the zonal wind. (three bottom panels) Differences in the time mean states of O_3, T, and U: dSfast-r, dMoz-r, and dMoz-i. The light and heavy shaded areas in grey colors indicate where the difference of the means is greater than 1-σ and 2-σ error bar. Contour interval is 5% for ozone difference, 0.5 K for temperature difference, and 0.5 m/sec for the zonal wind difference.

3. Impact of Uncertainty in O_2 Cross Sections on Stratospheric Climate

[15] The primary difference selected here is the model with reduced O_2 cross sections minus the model with standard cross sections:

dSfast-r = Sfast-O2jr minus Sfast-Ctrl,

dMoz-r = Mozart-O2jr minus Mozart-Ctrl.

The case with increased cross sections is reversed to make the primary changes comparable:

dMoz-i = Mozart-Ctrl minus Mozart-O2ji.

The maximum model difference in dMoz-i has about two thirds the magnitude of the other two for relative ozone and temperature changes.

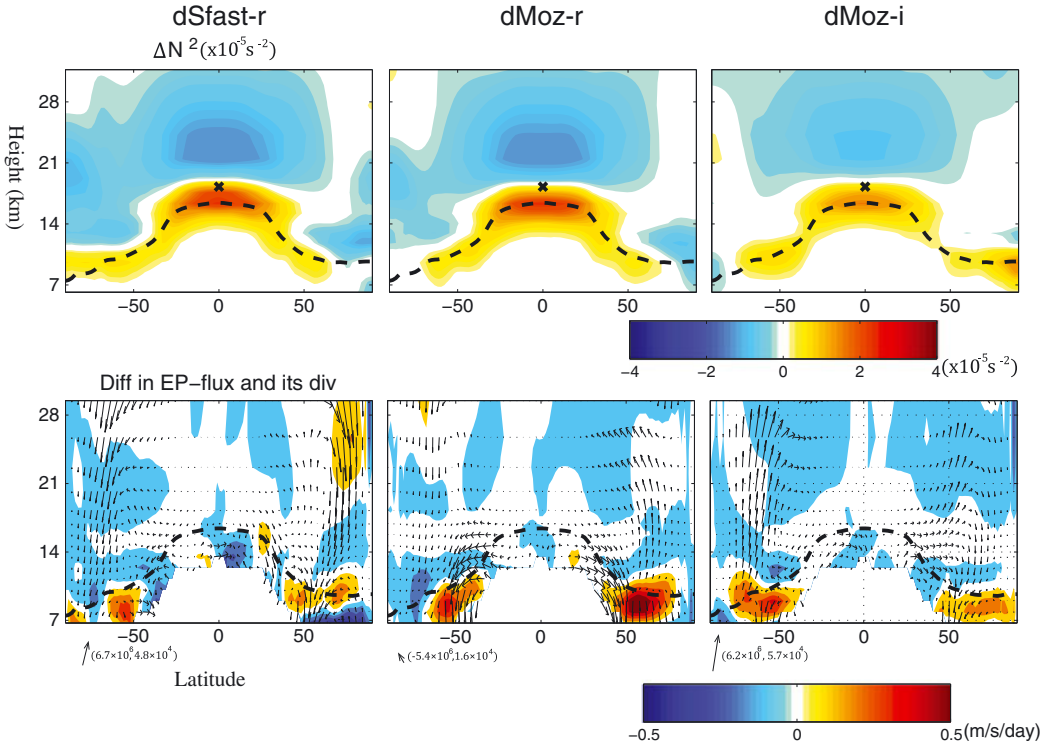

Figure 3. (top) Difference in time-mean buoyancy frequency squared (N^2) between the Sfast-O2jr and the Sfast-Ctrl, between Mozart-O2jr and Mozart-Ctrl, and between Mozart-Ctrl and Mozart-O2ji. (bottom) Difference in time-mean EP-flux and its divergence between runs corresponding to Figure 3, top. The X sign on Figure 3, top indicates the 72 hPa level. The dashed line indicates the mean tropopause for Mozart-Ctrl run. EP-fluxes are divided by the background air density ρ_o.

3.1. Impact on the Mean Climatology

[16] In this section we examine how the basic state of the stratosphere might change due to uncertainty in the O_3 photochemistry. Figure 2 shows the annually and zonally averaged distributions of ozone, temperature, and zonal wind for the Sfast-Ctrl as well as for the differences of these variables between the Mozart runs and Sfast runs. The basic state of the control run is similar to the current climate. The patterns of the differences reveal large-scale changes.

[17] The perturbed net ozone production (Figure 1a) drives a significantly different ozone distribution in CAM5. For both dSfast-r and dMoz-r, above the 30 hPa (∼24 km) level, the difference in ozone abundance changes gradually with altitude up to a maximum change of about –0.8 ppm in the top model layer, corresponding to a less than 10% decrease throughout the middle and upper stratosphere. Accompanied cooling over this region excluding high latitudes is consistent with the pattern of ozone change. Below 30 hPa, the difference in ozone abundance increases and reaches its maximum of about +0.25 ppm at a height of about 40 hPa (22 km). However, in terms of relative change, the maximum ozone increase is about 25–30% and occurs in the tropical lowermost stratosphere between 70-100 hPa (16–18.5 km). This is also where temperature changes the most, about 2 K, attributable to a slower radiative damping time scale in this region [*Randel et al.*, 2002]. Overall, the stratospheric temperature response pattern is consistent with a direct response to relative ozone change, except in high latitudes.

[18] The polar temperature responds quite differently for each paired experiment, and these temperature changes are not closely related to the in situ ozone heating. Colder polar temperatures are found in both hemispheres in dSfast-r, but a warmer Arctic region is seen in dMozart-r, and both poles are warmer in dMozart-i. As a result, changes in the mean zonal wind, related to the latitudinal temperature gradient, also differ in sign. Above 20 km, the changes in the zonal winds for dSfast-r are mostly westerly (positive), but turn more easterly (negative) in the tropical region for dMozart-r and are predominately easterly for dMozart-i. The only consistent change among these paired experiments is the deceleration of the subtropical westerly jets [*Haigh et al.*, 2005].

[19] We hypothesize that changes in the high-latitude temperatures are the result of changes in poleward eddy heat fluxes. Waves propagating from the troposphere that carry poleward heat flux are less likely to reach to the stratosphere if the vertical gradient of N^2 at the tropopause is enhanced [*Chen and Robinson*, 1992; *Simpson et al.*, 2009] and this can be caused by ozone heating [*Nakamura et al.*, 2009]. To illustrate this point, Figure 3 shows the differences in N^2, E-P fluxes divided by background air density, and its divergences for all three paired runs. Changes in N^2 for all cases exhibit a similar dipole structure with the positive maximum straddling over the tropopause and

a broad decrease in the lower stratosphere. The main difference across the cases is the poleward extension of the positive N^2 changes into high latitudes and its detailed structure at high latitudes. The hypothesis that the enhanced tropopause N^2 impedes upward wave propagation is well supported from the analyses of the mean difference in E-P fluxes. As seen in the figure, vectors representing changes in the E-P fluxes mostly point downward and thus indicate less poleward heat flux. Exceptions are where positive changes in the E-P flux divergence (warm colors in the bottom panels) extend considerably above the tropopause. At these places (NH high latitudes in dMoz-r and SH high latitudes in dMoz-i), waves are less absorbed and thus provide as a wave source anomaly to excite upward propagating waves. In dMoz-i between 40°N–50°N, waves are able tunnel through gaps of N^2 maxima and propagate upward. For all cases, the eddy heat flux anomalies are consistent with the mean temperature differences. That is, a colder polar vortex is a result of less poleward heat flux that occurs when the N^2 anomaly can effectively impede upward wave propagation.

[20] Although the vertical gradient of N^2 is only one term in computing the refractive index to map the path for linear wave propagation, it plays a crucial role regulating the upward propagating waves from the troposphere [*Chen and Robinson*, 1992]. For example, *Li et al.* [2007] showed that the vertical gradient of N^2 varies greatly in latitude, and it is essential to consider N^2 as function of latitude when computing the refractive index. One way to change the tropopause stability is through ozone heating [*Nakamura et al.*, 2009]. Here we find that the N^2 maximum anomaly at the tropopause from equator to midlatitudes is a consistent feature in all three cases due to ozone heating. However, the structures of N^2 at high latitudes and its effectiveness to impede wave propagation vary with model runs. This is because the polar temperature is controlled not only by radiative process but also by the internal dynamics of the atmosphere.

[21] The overall effect of different ozone chemistry on the annual-mean large-scale Brewer-Dobson circulation is negligible. For the monthly mean climatology of the winter and spring in both hemispheres, the mean meridional circulation changes by at most ±10% in magnitude through a change of eddy forcing in high latitudes. However, there are no consistent changes across dSfast-r, dMoz-r, and dMoz-i.

3.2. Impact on the Equatorial Annual and Semiannual Cycle

[22] In this section, we examine the equatorial annual and semiannual cycles simulated in CAM5 and explore if the perturbation of ozone production has any impact on these. The variation of the temperature in tropics exhibits a clear semiannual cycle above 30 hPa [*Reed*, 1962]. The mechanism driving the semiannual cycle has been associated with tropical planetary-scale Kelvin waves and small-scale gravity waves [*Garcia et al.*, 1997]. At solstice seasons, the direct solar heating of ozone can also theoretically drive a middle-atmosphere Hadley circulation in the upper stratosphere [*Dunkerton*, 1989] although the circulation is not realizable due to the inertial instability [*Shepherd*, 2000]. Below 50 hPa, however, the variation of temperature switches to a predominantly annual cycle in phase with the ozone annual cycle. The evidence of nearly compensating temperature variation between the tropics and the extratropics [*Yulaeva et al.*, 1994; *Ueyama and Wallace*, 2010] has been used to support the theory that ozone and temperature variations in the lower stratosphere merely follow the annual cycle of the wave-driven Brewer-Dobson circulation [*Randel et al.*, 2007]. However, the upwelling of the BDC cannot be the only factor for determining the annual cycle of ozone and temperature. In the lower stratosphere, ozone abundances are determined by photochemical production through the processes of O_2 photolysis, upwelling and lateral mixing from midlatitudes [*Avallone and Prather*, 1996; *Konopka et al.*, 2009]. For the temperature, the radiative heating, primarily through O_3, largely balances the adiabatic upwelling cooling and provides a net positive temperature tendency in the tropics for the NH summer [see *Rosenlof*, 1995, Figure 2a]. Recently, *Fueglistaler et al.* [2011] demonstrate that the residual of global net temperature variations is not as small as previously thought (a small residual implies the dynamical control of BDC). They show that ozone variation in the lowermost stratosphere amplifies the temperature signature in the tropical lower stratosphere to first order.

[23] Figures 4a–4c show the vertical profiles of the climatological seasonal cycle for ozone (O_3), temperature (T), and residual vertical velocity (w^*) of the Sfast-Ctrl over the deep tropics (10°N–10°S). The climatological seasonal cycles (thin lines) are obtained by averaging the data for each individual month. Anomalies (thick lines) are obtained by further removing the annual mean at each vertical level and are shaded in grey for negative values. Figures 4d–4i show the dSfast-r and dMoz-r climatological seasonal cycles for the same quantities. To emphasize the change in the lower stratosphere where O_3 abundances are small, we plot the change in ozone anomaly as a percentage of the total difference. For perspective, the typical anomaly magnitudes are in the range a few tens of parts-per-billion throughout the stratosphere for the O_3 difference, a few tenths of 1° for the T difference, and about 1 km/year for the w^* difference.

[24] The semiannual and annual cycle of O_3, T, and w^* are well simulated in the Sfast-Ctrl and are qualitatively similar in all other runs. A peak-to-peak amplitude of 8 K in the annual cycle of temperature at the 70 hPa (thick contours in Figure 4b) compares well with that in ERA-40 data in *Fueglistaler et al.* [2009, Figure 4]. The simulated w^* with the peak-to-peak magnitude of several kilometers per year, also has a prominent annual cycle in the lower stratosphere with the phase preceding the temperature and ozone by about a month in the lower stratosphere. As in calculations based on observed data [*Randel et al.*, 2007], we see a weakened residual vertical velocity followed by larger ozone abundances and a warmer lower stratosphere. As altitude increases, a semiannual cycle becomes more evident and most pronounced at the top model layer, i.e., ∼2 hPa.

[25] How do the annual or semiannual cycles change with the perturbation of ozone production? There are no consistent patterns in the anomaly differences across O_3, T, and w^* (e.g., comparing Figures 4d–4f for dSfast-r and Figures 4g–4i for dMoz-r). The anomaly difference for O_3 reveals a coherent semiannual cycle above 50 hPa, primarily following the insolation. The phase changes sign at around 25 hPa from compensating effects of opposite changes in overhead radiation (Figures 4d and 4g). A clean annual cycle

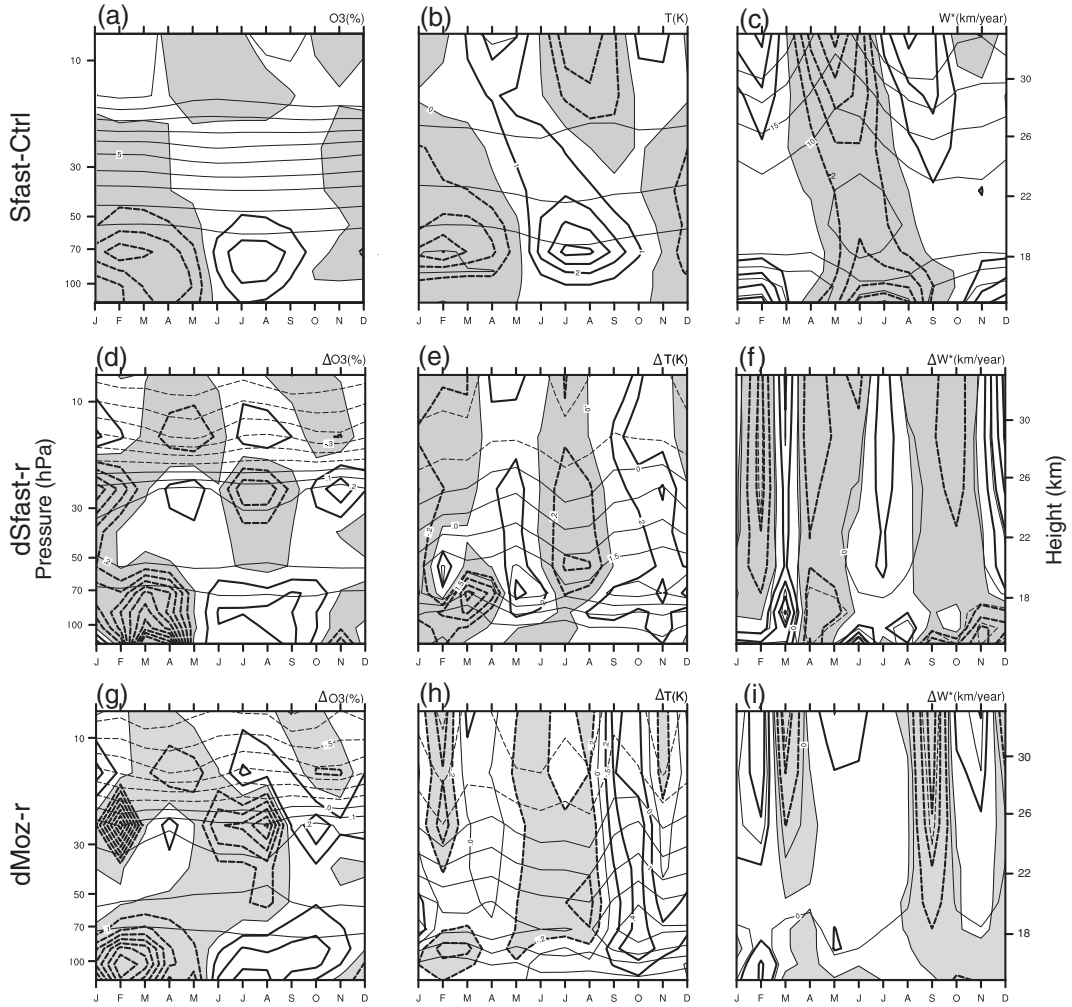

Figure 4. Zonally and time (10 year) averaged, monthly vertical profiles of (a) ozone (ppm) (b) temperature, T (K), and (c) residual vertical velocity, w^* (km/year) in the deep tropics of the stratosphere over 10°S–10°N. Thin contour lines are the monthly mean with contour interval of 1 ppm, 10 K, and 5,10,..,25,50,100 km/year respectively. Thick contour lines are anomalies with respect to the annual mean. Ozone anomalies are expressed as the percentage of the monthly mean with a contour interval of 10%. Anomaly contour interval for T and w^* is 1 K and 2 km/year, respectively. Negative anomaly values are shaded with dashed contour lines. Similar to Figures 4a–4c but for the differences from (d–f) dSfast-r and (g–i) dMoz-r. Thin lines are differences in the monthly mean with contour intervals of 0.1 ppm, 0.5 K, and 1 km/year. Thick lines are differences in anomalies with their respective annual mean removed. Difference in ozone anomaly is plotted as the percentage of the total difference with a contour interval of 10%. Contour interval for difference in T anomaly and w^* anomaly is 0.2 K and 0.5 km/year, respectively.

appears in absolute ozone in the lower stratosphere with the maximum amplitude at 70 hPa (not shown), and this pattern is qualitatively similar across dSfast-r, dMoz-r, and dMoz-i. This enhanced annual cycle is also apparent in the relative ozone change below 50 hPa as shown in Figures 4d and 4g. However, T and w^* anomaly differences are different across all three pairs (dMoz-i not shown). Above 50 hPa where the difference in w^* anomaly is most evident, the difference in T anomaly clearly follows w^* in dMoz-r, but that is not the case for dSfast-r, particularly for the months of January and February. For dSfast-r between 25 and 50 hPa, the T anomaly difference has a clear semiannual cycle in phase with the O_3 anomaly difference. Below 50 hPa, for dMoz-r, the w^* anomaly difference is negligible and thus the T anomaly difference is mostly associated with the annual cycle of the O_3 anomaly difference. In contrast, the local change in w^* in dSfast-r contributes partly to the larger T anomaly difference such as the maximum cooling seen in March.

[26] In conclusion, the seasonal response of ozone is qualitatively similar among the three sets of model experiments, but those of the temperature and residual circulation are dissimilar. This is partly because the residual circulation is wave driven and the basic climate of Mozart-Ctrl is quite different from that of Sfast-Ctrl. For example, the tropical waves triggered by convection are expected to be different since the cloud dynamics in Sfast is altered from the

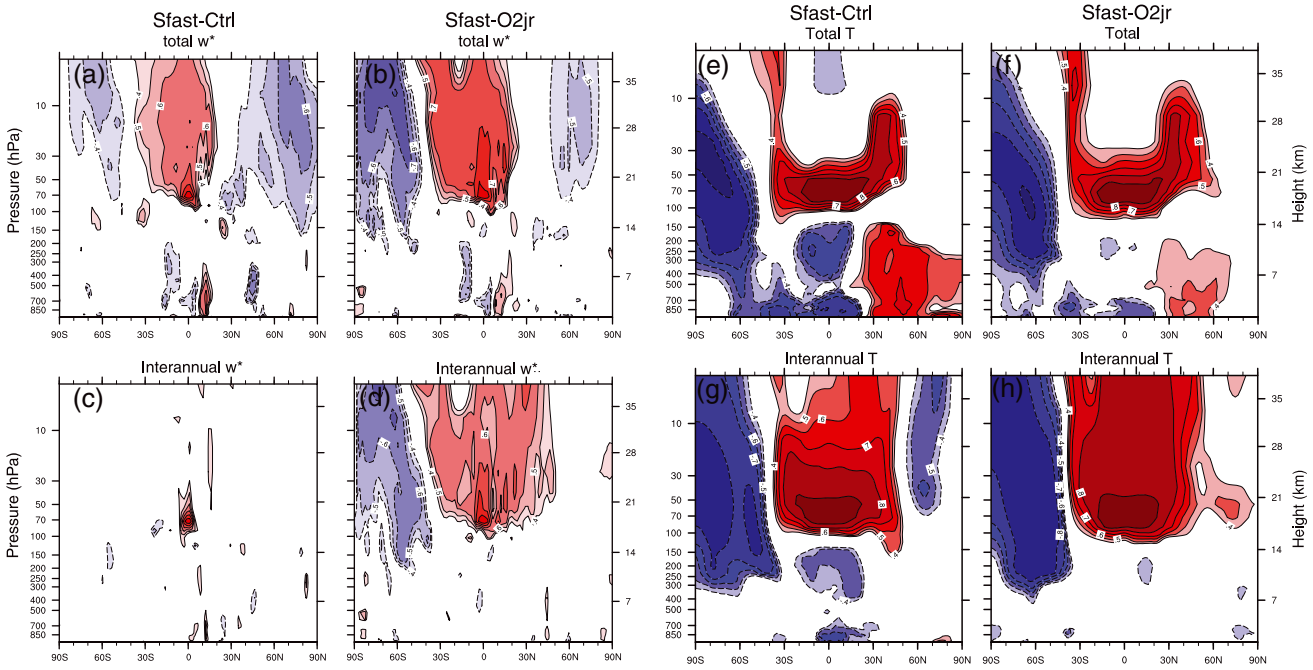

Figure 5. (a–d) One-point correlation map for JJA residual vertical velocity, w^* showing the correlation between the base point at (0°N, 72 hPa) with the rest of the model domain. Left column is for Sfast-Ctrl and right column is for Sfast-O2jr. (top) From monthly w^* time series. (bottom) Interannual JJA w^* components only. (e–h) Same as the Figures 5a–5d, but for temperature, T.

lack of the cloud-aerosol interactions. Furthermore, the basic time-mean BDC is faster in Mozart than in Sfast above 50 hPa. We speculate that in a faster circulation, the imprint of radiation from ozone is smaller. Thus, the T anomaly difference follows w^* more closely in dMoz-r than dSfast-r. Conversely, below the 50 hPa, the basic time-mean w^* in Mozart is considerably slower, and the effect of ozone on temperature through radiation is then more evident. Lastly, with the O_2 cross sections reduced, the prominent annual cycle of ozone anomaly is enhanced by about 10% at 70 hPa without corresponding enhancement of the annual cycle in w^*. This is because the ozone production from the reduced O_2 cross sections is more enhanced in a slower BDC season (JJA) than in a faster BDC season (DJF).

3.3. Impact on the Tropics and Extratropics Connections

[27] The 70 hPa level has been considered the upper boundary of the tropical tropopause layer [see *Fueglistaler et al.*, 2009, Figure 14] as well as the base of the residual circulation [*McLandress and Shepherd*, 2009]. The physical quantities at this level mostly reflect the characteristics of stratospheric radiative and dynamical processes, but tropical convective systems occasionally reach this level. In response to the 30% decrease in O_2 cross sections, the largest change is 2 K warming at 70 hPa. As a result, stratification is increased below this level but decreased above (see Figure 3).

[28] To investigate the impact of the warming, we show the time-correlation over the latitude-height domain of the mean residual vertical velocity w^* and temperature, T, to the base point at (0°N, 72 hPa). We expect to see a high anticorrelation between tropics and extratropics in residual vertical velocity, representing the BDC. If the temperature is mostly controlled by the BDC, we also expect to see a similar pattern. The one-point correlation procedure is applied by calculating the correlation coefficients between the JJA (or the DJF) time series (30 points = 10 years × 3 months for Sfast and 75 points = 25 years × 3 months for Mozart) between the base point and the rest of the grid points. We also repeat the same procedure after removing the climatological monthly mean for each month (e.g., July time series-July climatological mean, removing the component of the seasonal cycle) to examine the correlations for the interannual component. Here we present only the JJA results because they show a clear signal while the DJF patterns have no clear interpretation. We refer to the unfiltered monthly mean temperature as total T, and the filtered one with the seasonal cycle removed as interannual T.

[29] Figures 5a–5d show the JJA one-point correlation maps of w^* for Sfast-Ctr and Sfast-O2jr. Only correlation coefficients with $|\gamma| \geq 0.4$ are contoured. A coherent pattern with positive values (upwelling) in the tropics and negative values (downwelling) in high latitude appears for both runs. However, γ for the Sfast-Ctrl drops more quickly upward and remains less than 0.6 in the upwelling region (Figure 5a). The downwelling region has a weaker negative correlation (with γ between –0.4 and –0.5) for the SH high latitudes. In contrast, the extratropics for Sfast-O2jr is more synchronized with the tropics. Its correlation coefficient drops more slowly and remains at 0.7 for most of the upwelling region

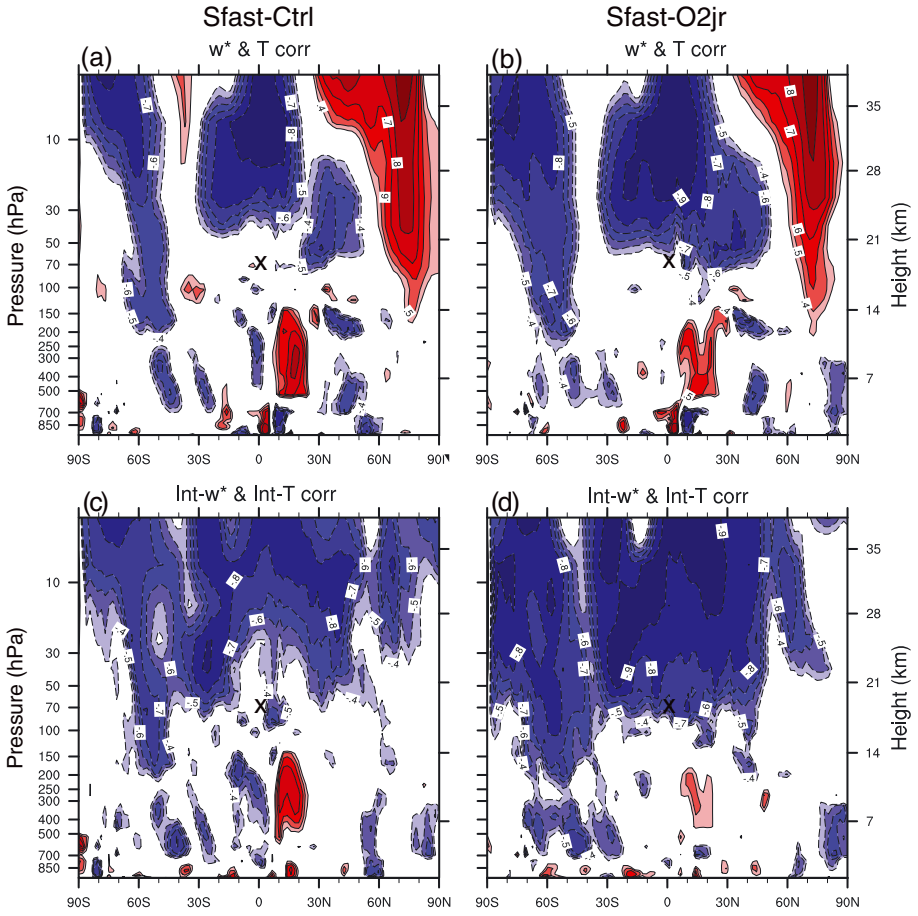

Figure 6. Cross-correlation maps between residual vertical velocity, w^*, and temperature, T, for JJA time series for (a, c) Sfast-Ctrl and (b, d) Sfast-O2jr. The layout and contours are the same as in Figure 5. The base point (0, 72 hPa) used in Figure 5 is marked as "x" for reference. Figures 6c and 6d are for interannual component only.

and has a stronger synchronized downwelling region (with γ between –0.6 and –0.7) in the SH high latitudes where the BDC is expected to be stronger during the austral winter (Figure 5b). Figures 5c and 5d show the same correlation maps but for the JJA interannual w^*. The striking feature of Sfast-Ctrl in Figure 5c is that the equatorial w^* at 72 hPa, is nearly uncorrelated ($|\gamma| < 0.4$) with other grid points showing that this point is isolated from the rest of the stratosphere. In contrast, for Sfast-O2jr, the correlation at this point to the SH decreases only slightly. In both runs, the anticorrelation to the NH high latitudes disappears reflecting that the NH summer BDC is weak or not present on a time scale longer than the seasonal cycle. The procedure is also repeated with the base point at 54 hPa or 38 hPa of the equator. Similar results are obtained with overall larger correlation values extending further into the upper stratosphere.

[30] Figures 5e–5h show the same one-point correlation but for T. T at 72 hPa, also the cold point temperature, is anticorrelated with T in the high latitude but mostly confined to the lower stratosphere compared to the corresponding w^* pattern. It is also highly correlated with that of the troposphere, but more so for the Ctrl run. For interannual T (Figures 5g and 5h), the correlation values increase, extend deeper to the upper stratosphere, and become less correlated to the troposphere. That the temperature correlation extends deeper to middle and upper stratosphere for interannual variability is also found in recent satellite data [*Young et al.*, 2011]. Note that, however, this is in contrast with the w^* analysis where the correlation is weakened after removing the seasonal cycle.

[31] To further relate the temporal variability in T to that in w^*, we compute the cross-correlation coefficients at each latitude-height grid point between total T and total w^* (Figures 6a and 6b) and also between their respective interannual components (Figures 6c and 6d). In general, for the winter hemisphere, there is an anticorrelation between T and w^* (i.e., upwelling is associated with adiabatic cooling and downwelling with adiabatic warming). This anticorrelation becomes slightly weaker in the upper stratosphere above 10 hPa but stronger elsewhere particularly in the subtropics after the seasonal cycle is removed (Figure 6c). Note that there is very little correlation ($|\gamma| \leq 0.4$) between w^* and T in the lower stratosphere in Figures 6a and 6c. This is in contrast with the see-saw pattern of T correlation maps seen in Figures 5e and 5g. In this example, the strong anticorrelation of T between tropics and high latitudes in the lower stratosphere does not represent the same variation by the BDC.

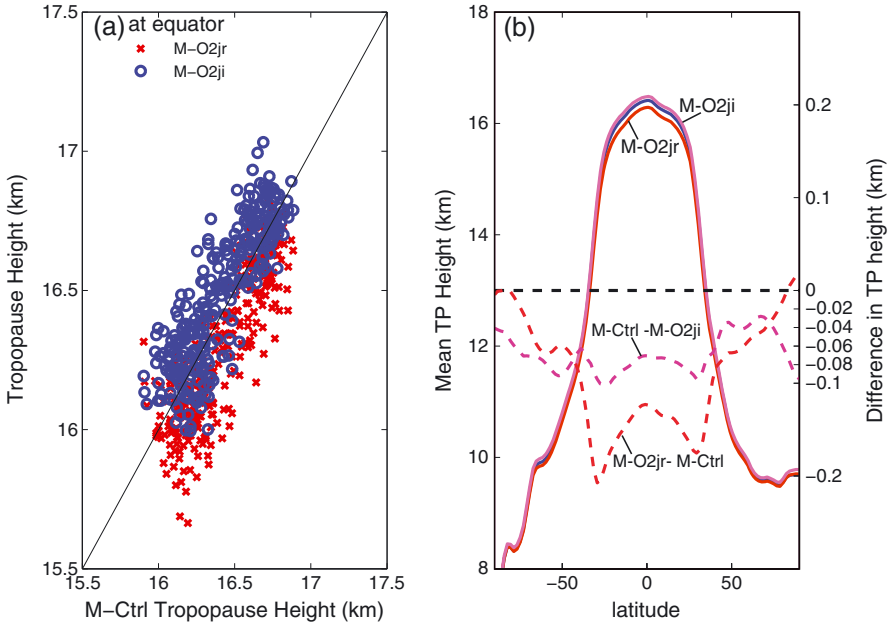

Figure 7. (a) Scatter plot for the monthly tropopause height between Mozart-Ctrl and Mozart-O2jr (red cross) and Mozart-Ctrl and Mozart-O2ji (blue circle). (b) The latitudinal distribution of the annual mean tropopause height for Mozart-Ctrl (blue line), Mozart-O2jr (red line), and Mozart-O2ji (magenta line) with values labeled on the left axis. The differences for dMoz-r and dMoz-i are labeled on the right axis.

[32] Total w^* and total T are poorly correlated in the tropical lower stratosphere in Sfast-Ctrl. The correlation slightly improves in the lower stratosphere when the monthly mean climatology is removed. But the improvement does not include the base point at (0°N, 72 hPa) marked as "x" for the Ctrl run. In contrast, the w^* and T are, in general, more correlated for Sfast-O2jr and even more so when the seasonal cycle is removed. We repeat the same calculations for the Mozart runs. Similar results are found in the pair of Mozart-O2ji versus Mozart-Ctrl but not in the pair of Mozart-Ctrl versus Mozart-O2jr.

[33] We hypothesize that in Sfast-Ctrl and Mozart-O2ji, the temperature near the 72 hPa at equator is more controlled by the tropical convection from below and less influenced by the wave forcing from midlatitudes through BDC (compare tropospheric patterns between Figures 5e and 5f). With the O_2 cross sections reduced, more ozone is created in the lower stratosphere. The radiative forcing of the ozone pushes down the tropopause and thus reduces the influence of tropical convection reaching to the base point. Figure 7a shows the monthly tropopause height distributions at equator for Mozart runs. Figure 7b shows the latitudinal distributions of the annual mean tropopause (left axis) and the corresponding differences in the annual mean tropopause height for dMoz-r and dMoz-i (right axis). Although the vertical resolution is coarse in CAM5, the differences in the tropopause heights are still distinguishable across Mozart runs and among Sfast runs (not shown). The annual mean tropopause height in the tropical region is lowered by ~ 0.15 km for dMoz-r, and 0.1 km for dMoz-i. Note that tropopause height is most affected in the subtropics.

[34] However, lowering the tropopause height does not necessarily increase the correlation of the chosen base point to the rest of the stratosphere as in dMoz-r (not shown). In Mozart-Ctrl, the base point at 72 hPa is already well-correlated or connected with the rest of the stratosphere and thus further lowering the tropopause in Mozart-O2jr does not further improve the "connectivity" of that point to the rest of the stratosphere. The possibility of the increased wave stress in the extratropics that helps pump more and deeper air mass out of the tropical upwelling zone is also considered. For example, there is a maximum positive change for w^* throughout the stratosphere in July for dSfast-r (Figure 4f). However, there is no apparent difference in the change of the eddy forcing or w^* for JJA when comparing dMoz-i and dMoz-r. Thus, changing the characteristics of the tropopause transition layer through ozone heating here is considered the more important factor for improving the ventilation of the lowermost stratosphere of the tropics.

3.4. Impact on High-Latitude Interannual Variability

[35] Polar vortices of the stratosphere are persistent cyclones with circumpolar westerly winds for most of the year, particularly strong in the winter season. Fluctuations of the polar vortices can be manifested in terms of the displacement of the vortex centers, the distortion of their shape, and their complete break-down [*Waugh and Randel*, 1999]. While the fluctuations are associated with the upward propagating planetary waves and wave breaking that originated from the troposphere, they in turn influence the surface climate [*Baldwin and Dunkerton*, 2005]. The NH variability of the polar vortex is usually larger and peaks in the winter months when the eddy forcing is strongest whereas the SH polar vortex is quieter in the winter months and the variability peaks in the austral spring [*Waugh and Polvani*, 2010].

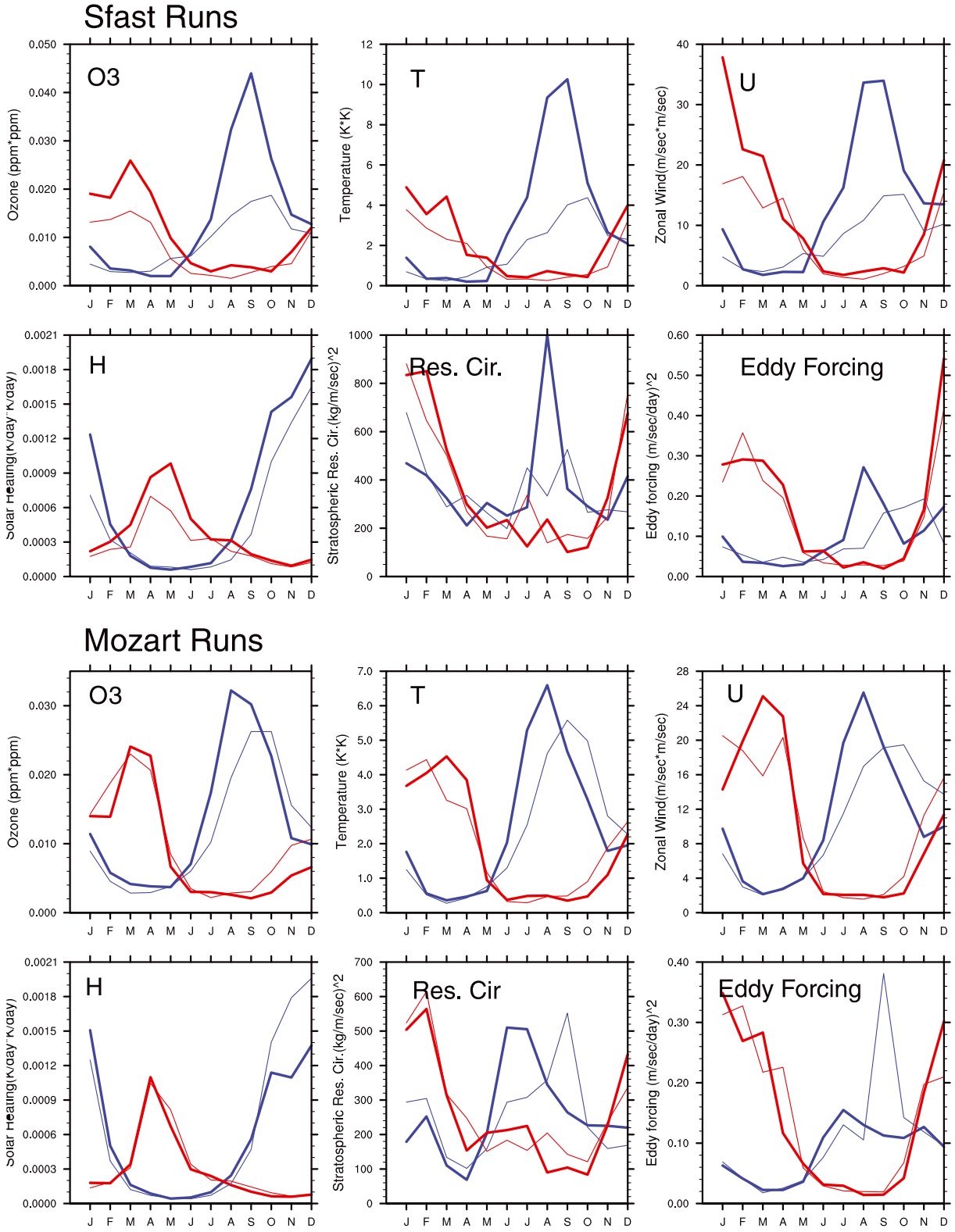

Figure 8. Total temporal variances averaged over the area-weighted stratospheric hemispheres from 120 hPa to 3 hPa. Blue lines are for the SH and red lines for the NH. Thick lines represent the O2jr run and thin lines the Ctrl run. Top six panels are from Sfast runs and bottom six panels from Mozart runs.

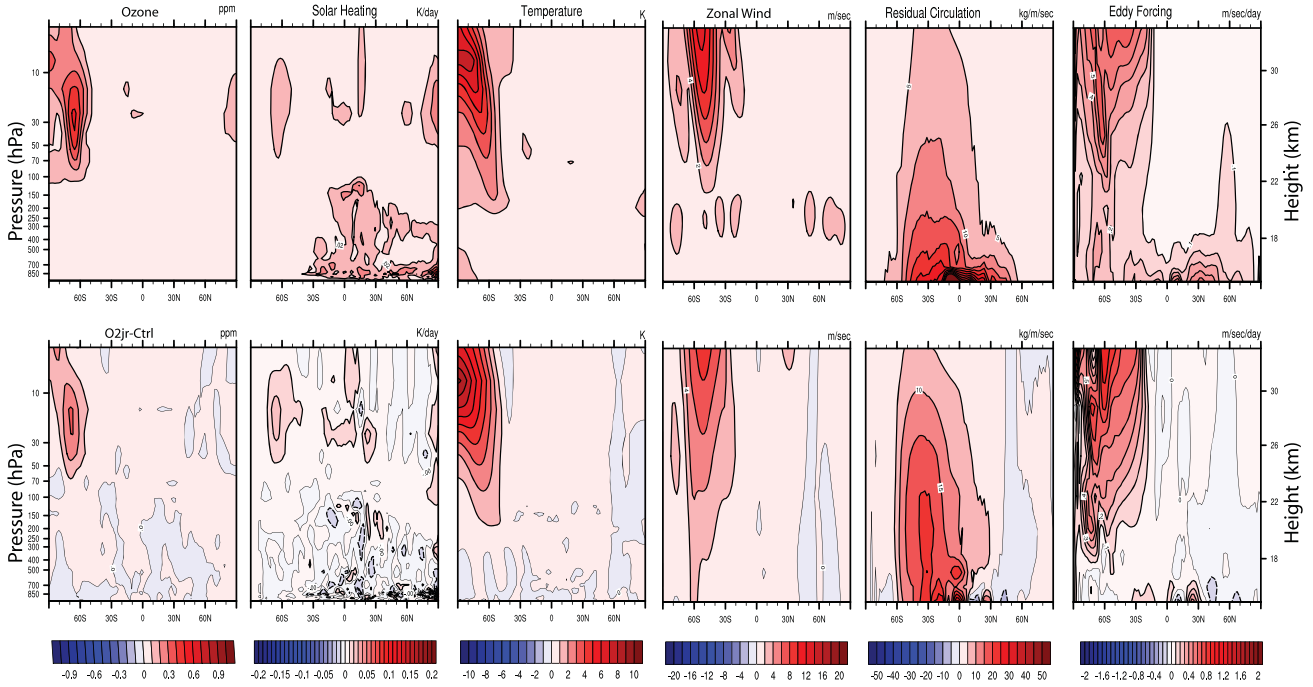

Figure 9. Latitude-height distributions of interannual variability expressed as the square root of the temporal variances for the month of August for (top) the Sfast-Ctrl run and (bottom) the differences between the Sfast-O2jr run and the Sfast-Ctrl run (dSfast-r).

[36] We have shown in section 3.1 that given the same forcing through change in O_2 cross sections, responses in the time-mean state of the polar vortices are different for each paired experiment depending on the amount of eddy poleward heat fluxes entering this area. The basic state zonal wind is one of the determining factors for upward wave propagation. Thus, when comparing changes in variability among these paired experiments, the characteristics of wave-mean flow interaction should be considered. Also, note that the model variances in these simulations are expected to be less than the observed or from full high-top atmosphere-ocean climate models because (1) El Niño–Southern Oscillation and other internal variation in SST, Quasi-Biannual Oscillation, volcanic eruptions, and solar cycles are not in the model and (2) the top of CAM5 only extends to 2 hPa [*Charlton-Perez et al.*, 2013].

[37] Figure 8 summarizes the temporal, area-weighted hemispheric variances of the six variables (ozone, temperature, zonal wind, solar heating, the mass stream functions, and eddy forcing) for Sfast and the corresponding Mozart runs. For both Ctrl runs, the NH interannual variability peaks in the extended winter months (DJFM) while the SH variability peaks during late winter and early spring (ASO). For Sfast-O2jr, increases in variability are seen in both NH and SH. The most evident change is the peak SH interannual variability (ASO) being shifted to late winter and early spring (JAS). For the Mozart pair, the NH variability has no significant change, and SH variability change is smaller compared to the Sfast pair. Nevertheless, the shift in SH peak variability from spring to late winter is still there.

[38] Figure 9 illustrates the latitude-height distribution of the mean interannual variability for the month of August, computed as the square root of the temporal variances for the six variables of Sfast-Ctrl and their differences from dSfast-r. In Sfast-Ctrl, the largest interannual variability in ozone, solar heating, and temperature occurs mostly over Antarctica, 60°S–90°S. The largest zonal wind variability is located slightly north of the polar vortex edge. From dSfast-r, variability is nearly doubled for all variables other than the solar heating. The increased variability of the eddy forcing penetrates deep into the SH polar vortex. Thus, the overall picture from dSfast-r consists of a more unsteady polar vortex with larger fluctuation in temperature and eddy forcing in the SH polar region.

[39] To evaluate the separation of the mean interannual variances between the Ctrl and O2jr runs, we modeled the probability density function (pdf) of the interannual time series of temperature variances (averaged over the grid points from 60°S–90°S and above 10 km) using the χ^2 distribution (as discussed in section 2.1). Figure 10 shows the mean and the standard deviation (vertical bar for each month) of the control parameter κ with the same unit of temperature variances, K^2, representing the best estimated mean temperature variances. Since the Mozart runs have 25 years of simulation and Sfast runs have only 10 years of simulation, we also repeat the same estimation by subsampling the Mozart time series into 16 ten successive years and the results are shown in Figure 10 (bottom). Given our simulated data, the variances of the temperature for the Sfast pair are well separated for the months of JAS for the southern hemisphere and the months of DJFM for the northern hemisphere. The separation of temperature variances is apparent only for SH September and NH March and April for Mozart pair. If these two pairs of experiments were identical, we might expect that the differences in variances would disappear if the simulations that are much longer than 25 years

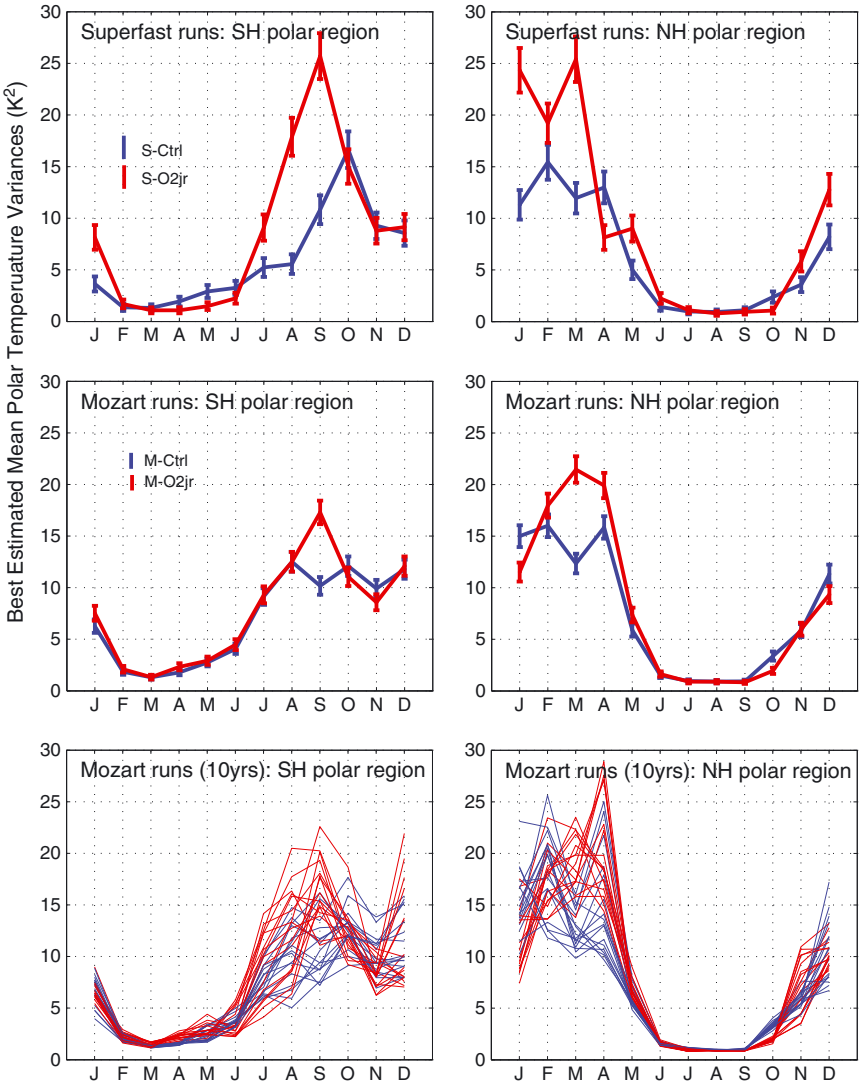

Figure 10. Best estimated values for the mean polar stratospheric temperature variances (poleward of 60° and above 10 km) from the Bayesian method.

were available. However, given that wave-mean flow interactions in high latitudes are played out differently in all pairs of runs and that Mozart-Ctrl and Sfast-Ctrl have very different basic climatology due to the difference in cloud-aerosol interaction scheme, the reduced difference in variances in Mozart pairs relative to Sfast pairs could be the result of a longer simulation but not necessarily so.

4. Conclusion and Discussion

[40] The impact of ozone photochemistry on climate through a 30% reduction in O_2 cross sections can be summarized as follows:

[41] 1. There is a large-scale temperature change, with opposite phases between the middle-upper and lower stratosphere in response to the change in ozone heating from the equator to midlatitudes. The maximum warming is 2 K.

[42] 2. Warming in the lowermost stratosphere changes the stratification of the atmosphere by increasing N^2 at the tropopause and decreasing N^2 in the stratosphere. The change in N^2 near the tropopause impedes the upward propagation of waves between about 60°S and 60°N. Changes in the mean polar temperatures are determined by eddy poleward heat fluxes rather than ozone heating.

[43] 3. There is an enhanced annual cycle of ozone but not of temperature or BDC in the tropical lowermost stratosphere. The temperature response in the lowermost stratosphere is the result of mixed influences from ozone heating and BDC.

[44] 4. Tropopause is lowered by about 100–200 m from radiative heating of ozone, consistent with the study of *Thuburn and Craig* [2000]. In Sfast-Ctrl (or Mozart-O2ji run), the air mass in the tropical lowermost stratosphere appears relatively isolated. With the tropopause lowered, a deeper BDC caused the lower stratosphere to be better ventilated.

[45] 5. The interannual variability increases for both hemisphere's winter. This is particularly evident for the austral winter during which the peak variability shifts toward late winter from early spring. However, the magnitude of

the increase as well as the shift, is not nearly as large in the longer simulation of Mozart-O2jr.

[46] *Haigh et al.* [2005] and *Simpson et al.* [2009] have shown that imposing a positive temperature perturbation in the lower stratosphere, to mimic solar variability, weakens the subtropical jets and Hadley cell. Though not a focus in this study, we also found that the subtropical jets and the Hadley cell are weakened in the simulations with reduced O_2 cross sections, showing that small changes in ozone photochemistry (within the uncertainty range) can influence the tropospheric climate as well.

[47] Perturbing Mozart-Ctrl and Sfast-Ctrl with the same forcing in ozone photochemistry does not produce the same responses in quantities such as the mean temperature of the polar region or the seasonal cycle of the temperature and residual vertical velocity because the responses of these quantities also depend on the basic state of the climate, wave sources in the troposphere, and wave-mean flow interactions. For example, Mozart-Ctrl relative to Sfast-Ctrl has a colder mean temperature by about 3 K below the tropical tropopause and a slower w^* with a warmer temperature by about 2 K in the lower tropical stratosphere. Consequently, Mozart-Ctrl has a more stratified mean state near the tropopause and thus the relative perturbation to the mean N^2 in dMoz-r is much smaller compared to dSfast-r. Future study with a finer vertical resolution near the tropopause, a fully resolved stratosphere and a systematic and larger increment in ozone forcing beyond the uncertainty range will further help quantify the climate responses due to changes in ozone photochemistry.

[48] **Acknowledgments.** We owe this project to a bet made many years ago between one author (M.J.P.) and J.R. Holton regarding ozone in the middle stratosphere. The observed latitudinal gradient of ozone from tropics to midlatitudes was generally flat while that of other chemical species like nitric acid was sharp, indicating a mixing barrier. Did the circulation respond to maintain this ozone flat gradient on the basis of heating gradients, or was it an accident? Here we found the latter. Jim was right; we miss you. This research was supported by the Office of Science (BER) and Lawrence Livermore National Laboratory (LLNL), U.S. Department of Energy under contracts DE-AC52-07NA27344, DE-AC02-05CH11231 (LLNL authors), and DE-SC0007021 (all authors). The numerical simulations were carried out using resources of the National Energy Research Scientific Computing Center (NERSC) at LLNL. J.H. would like to thank three anonymous reviewers for their comments and Francois Primeau for his help on the Bayesian statistics analysis.

References

Avallone, L. M., and M. J. Prather (1996), Photochemical evolution of ozone in the lower tropical stratosphere, *J. Geophys. Res.*, *101*(D1), 1457–1461, doi:10.1029/95JD03010.

Andrew, D., J. Holton, and C. Leovy (1987), *Middle Atmosphere Dynamics*, 481 pp., Academic Press Inc., London.

Baldwin, M. P. T., and J. Dunkerton (2005), The solar cycle and stratosphere-troposphere dynamical coupling, *J. Atmos. Sol. Terr. Phys.*, *67*(12), 71–82, ISSN 1364-6826, doi:10.1016/j.jastp.2004.07.018.

Cai, W., and T. Cowan (2007), Trends in southern hemisphere circulation in IPCC AR4 models over 1950–99: Ozone depletion versus greenhouse forcing, *J. Clim.*, *20*, 681–693, doi:10.1175/JCLI4028.1.

Cameron-Smith, P., J. F. Lamarque, P. Connell, C. Chuang, and F. Vitt (2006), Toward an Earth system model: Atmospheric chemistry, coupling, and petascale computing, in *Scidac 2006: Scientific Discovery through Advanced Computing,* vol. 46, edited by W. M. Tang, pp. 343–350, Institute of Physics, London, doi:10.1088/1742-6596/46/1/048.

Cariolle, D., A. Lasserre-Bigorry, J.-F. Royer, and J.-F. Geleyn (1990), A general circulation model simulation of the springtime Antarctic ozone decrease and its impact on mid-latitudes, *J. Geophys. Res.*, *95*(D2), 2156–2202, doi:10.1029/JD095iD02p01883.

Chen, P., and W. A. Robinson (1992), Propagation of planetary waves between the troposphere and stratosphere, *J. Atmos. Sci.*, *49*, 2533–2545, doi:10.1175/1520-0469(1992)049<2533:POPWBT>2.0.CO;2.

Charlton-Perez, A. J., et al. (2013), On the lack of stratospheric dynamical variability in low-top versions of the CMIP5 models, *J. Geophys. Res. Atmos.*, *118*, 2494–2505, doi:10.1002/jgrd.50125.

Dunkerton, T. (1989), Nonlinear Hadley circulation driven by asymmetric differential heating, *J. Atmos. Sci.*, *46*, 956–974.

Eyring, V., et al. (2006), Assessment of temperature, trace species, and ozone in chemistry-climate model simulations of the recent past, *J. Geophys. Res.*, *111*, D22308, doi:10.1029/2006JD007327.

Fueglistaler, S., A. E. Dessler, T. J. Dunkerton, I. Folkins, Q. Fu, and P. Mote (2009), Tropical tropopause layer, *Rev. Geophys.*, *47*, RG1004, doi:10.1029/2008RG000267.

Fueglistaler, S., P. Haynes, and P. M. Forster (2011), The annual cycle in lower stratospheric temperature revisited, *Atmos. Chem. Phys.*, *47*, 3701–3711, doi:10.5194/acp-11-3701-2011.

Froidevaux, L., et al. (2008), Validation of aura microwave limb sounder stratospheric ozone measurements, *J. Geophys. Res.*, *113*, D15S20, doi:10.1029/2007JD008771.

Garcia, R., T. J. Dunkerton, R. S. Lieberman, and R. A. Vincent (1997), Climatology of the semiannual oscillation of the tropical middle atmosphere, *J. Geophys. Res.*, *102*, 26019–26031.

Gettelman, A., J. E. Kay, and K. M. Shell (2012), The evolution of climate sensitivity and climate feedbacks in the community atmosphere model, *J. Clim.*, *25*, 1453–1469, doi:10.1175/JCLI-D-11-00197.1.

Haigh, J. D., M. Blackburn, and R. Day (2005), The response of tropospheric circulation to perturbations in lower-stratospheric temperature, *J. Clim.*, *18*, 3672–3685, doi:10.1175/JCLI3472.1.

Holton, J. R., P. Haynes, M. E. McIntyre, A. R. Douglass, R. B. Rood, and L. Pfister (1995), Stratosphere-troposphere exchange, *Rev. Geophys.*, *33*, 403–439.

Hsu, J., M. J. Prather, and O. Wild (2005), Diagnosing the stratosphere-to-troposphere flux of ozone in a chemistry transport model, *J. Geophy. Res. Atmos.*, *110*, D19305, doi:10.1029/2005JD005045.

Hsu, J., and M. J. Prather (2009), Stratospheric variability and tropospheric ozone, *J. Geophys. Res.*, *47*, D06102, doi:10.1029/2008JD010942.

IPCC (2007), in *Climate Change, the Physical Science Basis The Fourth Assessment Report of the Intergovernmental Panel on Climate Change*, edited by Solomon, S. et al., Cambridge University Press, Cambridge, U. K., 996 pp.

Konopka, P., J.-U. Groob, F. Ploger, and R. Muller (2009), Annual cycle of horizontal in-mixing into the lower tropical stratosphere, *J. Geophys. Res.*, *114*, D19111, doi:10.1029/2009JD011955.

Lamarque, J. F., et al. (2012), CAM-chem: Description and evaluation of interactive atmospheric chemistry in the Community Earth System Model, *Geosci. Model Dev.*, *5*(2), 369–411.

Lamarque, J. F., et al. (2013), The Atmospheric Chemistry and Climate Model Intercomparison Project (ACCMIP): Overview and description of models, simulations and climate diagnostics, *Geosci. Model Dev.*, *6*(1), 179–206, doi:10.5194/gmd-6-179-2013.

Lee, S., and S. B. Feldstein (2013), Detecting ozone-and greenhouse-gas-driven wind trends with observational data, *Science*, *339*(6119), 563–567, doi:10.1126/science.1225154.

Li, Q., H.-F. Graf, and M. A. Giorgetta (2007), Stationary planetary wave propagation in Northern Hemisphere winter climatological analysis of the refractive index, *Atmos. Chem. Phys.*, *7*, 183–200, doi:10.5194/acp-7-183-2007.

Li, F., J. Austin, and J. Wilson (2008), The strength of the Brewer-Dobson circulation in a changing climate: Coupled chemistry-climate model simulations, *J. Clim.*, *21*, 40–57, doi:10.1175/2007JCLI1663.1.

McLandress, C., and T. G. Shepherd (2009), Simulated anthropogenic changes in the Brewer-Dobson circulation, including its extension to high latitudes, *J. Clim.*, *114*, 1516–1534.

McLinden, C., S. Olsen, B. Hannegan, O. Wild, M. Prather, and J. Sundet (2000), Stratospheric ozone in 3-D models: A simple chemistry and the cross-tropopause flux, *J. Geophys. Res.*, *105*, 14,563–14,665.

Nakamura, T., H. Akiyoshi, and Y. Yamashita (2009), Influence of lower stratospheric ozone variation on tropospheric temperature and mean meridional circulation in the Northern Hemisphere summer, *Geophys. Res. Lett.*, *36*, L14701, doi:10.1029/2009GL038563.

Prather, M. (1992), Catastrophic loss of stratospheric ozone in dense volcanic clouds, *J. Geophys. Res.*, *97*(D9), 10,187–10,191.

Prather, M. (2009), Tropospheric O_3 from photolysis of O_2, *Geophys. Res. Lett.*, *36*, L03811, doi:10.1029/2008GL036851.

Randel, W. J., R. Garcia, and F. Wu (2002), Time-dependent upwelling in the tropical lower stratosphere estimated from the zonal-mean momentum budget, *J. Atmos. Sci.*, *59*, 2141–2152.

Randel, W. J., M. Park, F. Wu, and N. Livesey (2007), A large annual cycle in ozone above the tropical tropopause linked to the Brewer-Dobson circulation, *J. Atmos. Sci.*, *64*, 4479–4488, doi:10.1175/2007JAS2409.1.

Reed, R. (1962), Some features of the annual temperature regime in tropical stratosphere, *Mon. Weather Rev.*, *90*(6), 211–215.

Rosenlof, K. H. (1995), Seasonal cycle of the residual mean meridional circulation in the stratosphere, *J. Geophys. Res.*, *100*(D3), 5173–5191, doi:10.1029/94JD03122.

Rotman, D. A., et al. (2004), IMPACT, the LLNL 3-D global atmospheric chemical transport model for the combined troposphere and stratosphere: Model description and analysis of ozone and other trace gases, *J. Geophys. Res.*, *109*, D04303, doi:10.1029/2002JD003155.

Sander, S. P., et al. (2011), Chemical kinetics and photochemical data for use in atmospheric studies, Evaluation No. 17. Jet Propulsion Laboratory, Pasadena. http://jpldataeval.jpl.nasa.gov.

Schwartz, M. J., et al. (2008), Validation of the aura microwave limb sounder temperature and geopotential height measurements, *J. Geophys. Res.*, *113*, D15S11, doi:10.1029/2007JD008783.

Shepherd, T. (2000), The middle atmosphere, *J. Atmos. Sol. Terr. Phys.*, *62*, 1587–1601.

Simpson, I. R., M. Blackburn, and J. D. Haigh (2009), The role of eddies in driving tropospheric heating perturbations, *J. Atmos. Sci.*, *66*, 1347–1365, doi:10.1175/2008JAS2758.1.

Sivia, D. S., and J. Skilling (2006), *Data Analysis: A Bayesian Tutorial*, 2nd ed., 246 pp., Oxford Univ. Press, USA.

Stevenson, D. S., et al. (2013), Tropospheric ozone changes, radiative forcing and attribution to emissions in the Atmospheric Chemistry and Climate Model Intercomparison Project (ACCMIP), *Atmos. Chem. Phys.*, *13*(6), 3063–3085.

Tang, Q., and M. J. Prather (2012), Five blind men and the elephant: What can the NASA Aura ozone measurements tell us about stratosphere-troposphere exchange?, *Atmos. Chem. Phys.*, *12*, 2357–2380, doi:10.5194/acp-12-2357-2012.

Tang, Q., and M. J. Prather (2010), Correlating tropospheric column ozone with tropopause folds: The Aura-OMI satellite data, *Atmos. Chem. Phys.*, *10*, 9581–9688.

Thuburn, J., and G. Craig (2000), Stratospheric influence on tropopause height: The radiative constraint, *J. Atmos. Sci.*, *57*, 1728.

Ueyama, R., and J. M. Wallace (2010), To what extent does high-latitude forcing drive tropical upwelling in the Brewer-Dobson circulation?, *J. Atmos. Sci.*, *67*, 1232–1246.

Waugh, D. W., and W. J. Randel (1999), Climatology of arctic and antarctic polar vortices using elliptical diagnostics, *J. Atmos. Sci.*, *56*, 1594–1613, doi:10.1175/1520-0469(1999)056<1594:COAAAP>2.0.CO;2.

Waugh, D. W., F. Primeau, T. DeVries, and M. Holzer (2013), Recent changes in the ventilation of the southern oceans, *Science*, *339*(6119), 568–570, doi:10.1126/science.1225411.

Waugh, D. W., and L. M. Polvani (2010), Stratospheric polar vortices, in *The Stratosphere: Dynamics, Chemistry, and Transport, Geophys. Monogr. Ser.,* vol. 190, edited by L. M. Polvani, A. H. Sobel, and D. W. Waugh, pp. 43–57, AGU, Washington, D. C.

Yoshino, K., et al. (1988), Improved absorption cross-sections of oxygen in the wavelength region 205–240 nm of the Herzberg continuum, *Planet. Space Sci.*, *36*(12), 1469–1475.

Young, P. J., D. W. J. Thompson, K. H. Rosenlof, S. Solomon, and J.-F. Lamarque (2011), The seasonal cycle and interannual variability in stratospheric temperatures and links to the Brewer-Dobson circulation: An analysis of MSU and SSU data, *J. Clim.*, *24*, 6243–6258, doi:10.1175/JCLI-D-10-05028.1.

Yulaeva, E., J. Holton, and J. Wallace (1994), On the cause of the annual cycle in tropical lower-stratospheric temperatures, *J. Atmos. Sci.*, *51*, 169–174.